5-2010

The Mechanical Properties of Single Fibrin Fibers

W. Liu

Christine C. Helms
University of Richmond, chelms@richmond.edu

E. A. Sparks

Martin Guthold

The mechanical properties of single fibrin fibers

W. Liu[*], C. R. Carlisle[*], E. A. Sparks[*] and M. Guthold[*†]

[*]Dept. of Physics, 7507 Reynolda Station, Wake Forest University, Winston-Salem, NC 27109

W. Liu and C. R. Carlisle contributed equally to this manuscript

[†]To whom correspondence should be addressed:

Martin Guthold

Department of Physics

7507 Reynolda Station

Wake Forest University

Winston-Salem, NC 27109

Phone: 336-758-4977

Fax: 336-758-6142

E-mail: gutholdm@wfu.edu

Section heading: Coagulation

Abstract

Background. Blood clots perform the mechanical task of stemming the flow of blood.

Objectives. To advance understanding and realistic modeling of blood clot behavior we determined the mechanical properties of the major structural component of blood clots, fibrin fibers.

Methods. We used a combined atomic force microscopy (AFM)/fluorescence microscopy technique to determine key mechanical properties of single crosslinked and uncrosslinked fibrin fibers.

Results and Conclusions. Overall, full crosslinking renders fibers less extensible, stiffer, and less elastic than their uncrosslinked counterparts. All fibers showed stress relaxation behavior (time-dependent weakening) with a fast and a slow relaxation time, 2 s and 52 s.

In detail, crosslinked and uncrosslinked fibrin fibers can be stretched to 2.5 and 3.3 times their original length before rupturing. Crosslinking increased the stiffness of fibers by a factor of 2, as the total elastic modulus, E_0, increased from 3.9 MPa to 8.0 MPa and the relaxed, elastic modulus, E_∞, increased from 1.9 MPa to 4.0 MPa upon crosslinking. Moreover, fibers stiffened with increasing strain (strain hardening), as E_0 increased by a factor of 1.9 (crosslinked) and 3.0 (uncrosslinked) at strains $\varepsilon>110\%$. At low strains, the portion of dissipated energy per stretch cycle was small (<10%) for uncrosslinked fibers, but significant (~ 40%) for crosslinked fibers. At strains greater than 100%, all fiber types dissipated about 70% of the input energy.

We propose a molecular model to explain our data. Our single fiber data can now also be used to construct a realistic, mechanical model of a fibrin network.

Keywords: Atomic Force Microscopy (AFM), fluorescence microscopy, mechanical properties, single fibrin fibers.

Introduction

Blood clots have the essential mechanical task of stemming the flow of blood, and for the past six decades there has been continuing interest in resolving the mechanical properties of clots and their constituents [1]. The importance of the mechanical properties of a clot is underscored by the fact that they can be related to clotting disorders and disease [2, 3]. Properties of the whole, macroscopic clot can be determined via rheometry [3-6]. Moreover, single molecule experiments [7] and the known X-ray structure of fibrinogen provide molecular information [8]. A combination of rheometry, electronmicroscopy and small angle X-ray diffraction, has recently also been used to investigate the multiscale mechanical behavior of fibrin polymers [6], suggesting that protein unfolding plays an important role at the molecular scale, while fiber stretching and fiber alingment play key roles at the meso- and macroscopic scales. However, single fiber properties that connect underlying molecular mechanisms and macroscopic mechanical properties of a clot, have only recently started to emerge, and their understanding remains far from complete [1]. This single fiber knowledge is critical for constructing mechanical models of clots and, thus, deeper understanding of clot behavior [1, 6].

Blood clots are formed when soluble fibrinogen is converted to fibrin monomers that polymerize to form a network of fibrin fibers. The network is further stabilized by the formation of covalent bonds (crosslinks) between specific glutamine and lysine residues of the fibrin monomers [3]. It is this branched network of fibrin fibers that mostly determines the mechanical properties of a clot. Generally, the mechanical properties of such a network depend on three network properties [9, 10]: 1) the network architecture which describes the overall structural composition of the

network; 2) the mechanical properties of the individual fibers that comprise the network; 3) the properties of the joints between fibers. The architecture of the fibrin network may be determined from microscopy images [3]. However, beside the extensibility and elastic limit [11], the elastic modulus for small strains [12] and the rupture force of dried fibrin fibers [13], the mechanical properties of single fibrin fibers are unknown. Yet, exactly this knowledge on the single fiber level is needed to construct and test mechanical models of clots and, thus, advance our understanding of clot mechanical behavior [1, 6, 9, 10]. The mechanical properties of fibrin fibers are among the crucial factors that determine if a clot will deform, rupture or embolize. Considering the fact that blood clots *can* embolize, it is clear that physiological blood flow can create a large enough force to deform and rupture fibrin fibers.

We have developed a combined AFM/fluorescence microscopy technique to determine the mechanical properties of individual nanoscopic fibers [14]. We have collected stress-strain (force-extension) curves over the entire, extraordinarily large extensibility range of crosslinked and uncrosslinked fibrin fibers and report their distinct mechanial behavior. We have determined the i) extensibility (stretchability); ii) elasticity; iii) strain hardening behavior (stiffening with increased stretching), iv) energetic behavior (dissipated and stored energy); v) total and vi) relaxed elastic modulus (viscoelastic stiffness), and vii) stress relaxation behavior (time-dependent behavior). We propose a molecular model, based on two major secondary structure transformations and an extension of the interacting αC regions of the fibrin monomer, to explain the observed mechanical behavior.

Materials and Methods

Fibrin fiber formation. Uncrosslinked and crosslinked fluorescently labeled fibrin fibers were formed on a striated substrate made from cured optical adhesive (details, supplement). All experiments were carried out in "fibrin buffer" (140 mM NaCl, 10 mM Hepes, 5 mM $CaCl_2$, pH 7.4). For each experiment, two samples were prepared in parallel. One sample was used for the AFM manipulation experiments, the other for SDS PAGE. Crosslinked samples showed complete γ–γ and α–α crosslinking ($\geq$ 90%), while the samples without added Factor XIII showed no crosslinking.

Manipulation of fibers. The mechanical manipulations on fibrin fibers were performed with a combined AFM/optical microscope instrument (details, supplement). The schematic set-up is shown in Figure 1 A & B. The instrument is based on a Zeiss inverted optical microscope, a Hamamatsu, high sensitivity camera and a Topometrix Explorer AFM. The microscope stage was designed so that the AFM tip, fiber sample and objective lens can move with respect to each other, which allows alignment of the fiber with the AFM tip and objective lens. The AFM manipulation experiments were done with a nanoManipulator, a software program that interfaces the AFM with a force feedback stylus and a graphics computer [15]. The nanoManipulator provides control over the x-, y- and z-movement of the AFM tip. The AFM tip is used to stretch the fibrin fibers that are suspended across 12 μm wide channels in the striated, transparent substrate. The fluorescence microscope, situated underneath the substrate is used to collect movies of this stretching process (for movies, see supplement). The extension of the fiber was

determined by fluorescence microscopy and calculation using the distance traveled by the AFM tip (Fig. 1B). The applied force was determined from the twist of the cantilever. The force measurements were calibrated via the Sader method [16] and the Liu method [17].

Results

Stress-strain curves. For manipulations, we selected single fibers bridging the grooves in a straight line approximately perpendicular to the ridge edge. We have found that most fibers are well-anchored on the ridges of the striated substrate, even at extreme fiber extensions. We excluded fibers that slipped on the ridges from our analysis. This experimental design yields a well-defined geometry to determine the mechanical properties of fibrin fibers (Fig. 1 A & B).

The mechanical properties of polymers are generally determined via stress-strain (force-extension) curves in which stress, σ, is plotted as a function of strain (deformation), ε, under a variety of conditions. For longitudinal stretching experiments, as done here, stress is defined as F/A, where F is the applied force and A is the *initial* cross-sectional area of the stretched polymer. This is the definition of the commonly used *engineering stress*, which uses the initial cross-section and does not consider how the cross-sectional area changes as ε increases. Engineering stress gives a lower limit for the stress applied to the polymer, since the cross-sectional area most likely decreases as the fiber is stretched. Strain is defined as $\Delta L/L_{init}$, or $(\Delta L/L_{init})\cdot 100\%$, where ΔL is the change in length and L_{init} is the initial length. A typical stress-strain curve of a fibrin fiber being stretched to 1.75 times its initial length, ($\varepsilon = 0.75$ or 75%), is shown in Figure 1C.

The forward and return paths do not overlap; this means that energy (proportional to area under curves) is lost in this stretching cycle. However, although energy is lost, there is no permanent lengthening of the fiber (σ on return path does not reach 0 until $\varepsilon = 0$). The energy loss is due to the viscous properties of fibrin fibers and it is an indication that fibrin fibers are *viscoelastic* polymers. The slope of this curve corresponds to the stiffness (modulus) of the fiber, here about 1.3 MPa. However, it is apparent that such a simple analysis of just the slope misses some key properties of the fiber, such as its viscoelasticity, energy loss, and stiffening with increasing strain. In our experiments we analyzed basic and viscoelastic mechanical properties. A typical movie sequence of a fibrin fiber stretching experiment is shown in Figure 1D–F (movies and additional data, see supplement).

Fibrin Extensibility and Elastic Limit. Previously, fibrin fiber extensibility, ε_{max}, defined as the strain (extension) at which fibers rupture, was determined to be 333% and 226% for partially crosslinked and uncrosslinked fibrin fibers, respectively [11]. The elastic limit, $\varepsilon_{elastic}$, defined as the largest strain to which fibers can be stretched and recover to their original length without visible permanent deformation, was previously determined to be 180% and 120% for partially crosslinked and uncrosslinked fibrin fibers [11]. It is important to note, that the fibers in this previous study were only partially crosslinked. Here, we determined the extensibility and elastic limit of *fully* crosslinked fibrin fibers. ε_{max} was 147%, which is lower than both partially crosslinked and uncrosslinked fibrin fibers. We found the elastic limit of fully crosslinked fibers to be less than 50% strain. For a few manipulations, the elastic limit was 50% strain; however,

many fibers showed permanent deformation at strains as low as 10% (see movie in supplement). All mechanical properties of crosslinked and uncrosslinked fibers are summarized in table 1; table S1 in the supplement also includes all the data for *partially* crosslinked fibers.

Strain hardening. Strain hardening refers to the phenomenon when the elastic modulus (stiffness, slope of the stress-strain curve) increases (hardens) with increasing strain. We observed strain hardening, occurring at approximately 100% strain, for all fibrin fibers. However, crosslinked and uncrosslinked fibers do display several differences: Uncrosslinked fibers are initially softer; they show larger extensibilities and significant strain hardening. Crosslinked fibers are initially stiffer, show less extensibility and show less pronounced strain hardening. In Figure 2A, a stress-strain curve of an uncrosslinked fibrin fiber is plotted. In Figure 2B the total elastic modulus, E_0, i.e. the *slope* of the forward stress-strain curve in Figure 2A, is plotted as a function of strain. The curve displays a distinct sigmoidal shape; the total elastic modulus is relatively constant for the first 100% of strain; it then increases by a factor of about 3 and then remains at this higher value until the fiber ruptures. The strain hardening factor, h, i.e. the average ratio of the total elastic modulus at large strain (at $\varepsilon > 110\%$) to that at small strain ($\varepsilon < 80\%$) are listed in Table 1. On average, uncrosslinked fibers harden by a factor of 3.0 ($p \leq 0.0008$). A strain hardening factor of 1.9 ($p \leq 0.049$) was determined for crosslinked fibers. However, while crosslinked fibers did show significant strain hardening, as indicated by t-test analysis, hardening occurred with less consistency. Figure 2C shows a crosslinked fibrin fiber, stretched to 130%, which does not show strain hardening.

Stored and dissipated energy per stretch cycle. As seen in Fig 1C, not all of the energy put into stretching a fibrin fiber (area under forward stress-strain curve) is stored. A fraction of this energy is lost (dissipated) due to viscous processes. The dissipated energy is proportional to the area inscribed by the forward and backward curves. We have determined the amount of dissipated energy per stretch cycle as a function of strain (Figure 3). Uncrosslinked fibers show little energy loss at low strains and 70% energy loss at high strains. Crosslinked fibers already show significant energy loss at low strains.

Figure 3A shows three pulling cycles on the same uncrosslinked fibrin fiber with strains of 48%, 85% and 125%, respectively. It can be seen that the fiber dissipated almost no energy (all energy is stored) in the first pull ($\varepsilon = 48\%$), as the area between the forward and backward curve is very small. However, for larger strains ($\varepsilon = 85\%$ and $\varepsilon = 125\%$) a significant fraction (28% and 43%, respectively) of the energy is dissipated. It should be noted that even though large amounts of energy are dissipated, uncrosslinked fibers still return to their original length, meaning that they did *not* permanently lengthen, at strains less than 120% [11].

In Figure 3B, the ratio (percentage) of dissipated energy to the total energy is plotted as a function of strain. The graph for uncrosslinked fibers shows a clear sigmoidal shape. The energy loss at low strains is very small; it then increases significantly at strains between 50%-100% and remains at a constant, higher energy loss level of around 70% for larger strain.

Conversely, crosslinked fibers showed significant energy loss at low strains (43% energy loss for small strains of $\varepsilon < 40\%$). At larger strains ($\varepsilon > 40\%$), the energy loss increased to a plateau of 70% at 100% strain. This increased energy loss (at low strains) for crosslinked fibers is consistent with the notion that crosslinked fibers undergo permanent deformation at much lower strains ($\varepsilon_{elastic} < 50\%$) than uncrosslinked fibers.

Total and relaxed elastic moduli (fiber stiffness). Both uncrosslinked and crosslinked fibrin fibers show clear viscoelastic (time-dependent) behavior. We also found that crosslinking increases the stiffness (total and relaxed elastic modulus) by a factor of 2.

Incremental stress-strain curves [18], are a technique to separate the elastic (energy stored) and viscous (energy lost) components in viscoelastic materials (Fig. 4). In this technique, the fiber is stretched to a certain strain, where it is held constant for some time. Due to viscous processes, the fiber relaxes; that is, the force (stress) to hold it at that strain decreases. Subsequently, the fiber is stretched by another increment and held at constant strain. Again, the fiber relaxes and the stress decreases. This incremental straining is repeated several times. Figure 4A shows the strain vs. time curve of a fibrin fiber; the fiber was incrementally stretched to 23%, 46%, 75%, 104% and 138% strain and held constant at those strains for about 120 s. Figure 4B shows the corresponding stress vs. time curve of this fiber and it is readily apparent that the fiber relaxes (stress decreases) at each constant strain value. The x-axis (time) in Figure 4A and B are the same. The stress does not decay to zero, but to a constant value at each strain. When plotting each of the peak stress values vs. strain and the relaxed stress values vs. strain, the stress-strain

curves in Figure 4C are obtained. The relaxed stress values, σ_∞ for $t \rightarrow \infty$ were obtained by fitting two exponentials (details, see supplement). The slope of the higher curve in Figure 4C is the total elastic modulus, E_0, obtained before relaxation, and the slope of the lower curve is the relaxed, elastic modulus, E_∞, of fibrin fibers, obtained for $t \rightarrow \infty$. For crosslinked fibers, E_0 was 8.0 MPa, and E_∞, was 4.0 MPa. For uncrosslinked fibers, E_0 was 3.9 MPa and E_∞ was 1.9 MPa. Somewhat simplistically speaking, E_0 corresponds to the stiffness of the fibers when they are pulled fast; and E_∞ when they are pulled slowly. For comparison, other materials with stiffness in the MPa range are elastin fibers, spider silk, or a soft rubber band [19].

Stress relaxation. Stress relaxation, as seen in Fig. 4B, is indicative of viscous (time-dependent) processes [5]. Stress relaxation curves are usually fitted with one or more exponential functions yielding stress relaxation times. We have done an analysis of the stress relaxation behavior of fibrin fibers using a generalized Kelvin model (see supplement). Both crosslinked and uncrosslinked fibers show two stress relaxation rates; a fast (2 s to 4 s) and a slow relaxation rate (49 s to 57 s). These two rates are indicative of two distinct molecular relaxation processes, such as a molecular unfolding or transformation event, occurring with these time scales.

Discussion

We have investigated the mechanical properties of single crosslinked and uncrosslinked fibrin fibers. All our findings are summarized in table 1 (and table S1, which includes the data for partially crosslinked fibers).

Our values for the total elastic modulus, E_0, for uncrosslinked and crosslinked fibers (3.9 and 8.0 MPa) agree to within a factor of 2 with the small strain values obtained by Collet et al. (1.7 and 14.5 MPa) as determined by laser tweezers [12]. The differences may be explained by the different experimental set-ups and inherent, instrumentation-related errors.

The force *per fibrin monomer* can also be estimated from our data and compared with single protein unfolding experiments (calculations, see supplement). From our data, the force per monomer at 100% strain is about 140 pN, which is consistent with the 100 pN force to stretch a single fibrin monomer by 100% found by Brown et al. [7]. From our data, the rupture force per monomer is about 280 pN, which is similar to the 260 pN (2·130 pN) required to rupture the two A:a interactions between half-staggered monomers within a protofibril [20]. Interestingly, these forces are smaller than some protein unfolding forces [21], suggesting that some regions of the fibrin monomer may unfold *before* the fiber ruptures.

The energy per monomer required to rupture the fiber, as obtained from the area under our stress-strain curves (2400 kJ/mol) is of the same order of magnitude as the melting enthalpy of fibrin molecules (4650 kJ/mol) [22] (calculations, see supplement), again indicating that fibrin may melt (denature), before the fiber ruptures.

Crosslinking had a significant and intriguing effect on several mechanical properties, and no effect on other properties. Uncrosslinked fibrin fibers are very extensible, are elastic at high strains, are relatively soft, show strain hardening by a factor of 3.0, and a sigmoidal energy loss curve going from 0% loss at low strains to 70% loss at high strains. Complete crosslinking makes fibers stiffer, less extensible, more susceptible to plastic deformation at a lower strain, and increased the low-strain energy loss. Being already stiffer, crosslinked fibrin fibers did not show the same amount of strain hardening and often did not extend to strains at which strain hardening would have occurred. γ–γ crosslinks form between two reciprocal sites on the abutting γ-nodules of aligned fibrin monomers within a protofibril, and they are thought to be oriented along the longitudinal fiber axis. α–α crosslinks form between numerous sites on the extensive, flexible and partially unstructured αC regions (α221-610), and due to the length of this domain they may be oriented in the lateral (radial direction), and longitudinal direction. In previous experiments, partially crosslinked fibrin showed the largest extensibility (330%) [11]. Thus, crosslinking seems to have a bell-shaped effect on extensibility; from $\varepsilon_{max} \sim 230\%$ (uncrosslinked) to $\varepsilon_{max} \sim 330\%$ (partial crosslinking) to $\varepsilon_{max} \sim 150\%$ (fully crosslinked). Full crosslinking appears to have a restricting effect on previously mobile regions (e.g. the αC regions), it may prevent unfolding of domains and/or it might tighten the fibrin monomer and protofibril interactions.

Clot rheology studies on *whole clots* showed that crosslinking induces a 2 to 3.5-fold increase of rigidity [3, 23, 24] of the whole clot, which is similar to the 2-fold increase in E_0 of single fibers we observed.

To explain the observed mechanical behavior of fibrin fibers, we propose a model with the following three molecular mechanisms (Fig. 5). The mechanisms may occur in parallel as the fibers are stretched. 1) α-helix to β-strand conversion of the two coiled coils of the fibrin monomer. This conversion can account for 90 – 100% strain [7, 19]. 2) Deformation or partial unfolding of the γ-nodule of the fibrin monomer. This conversion may account for an additional 220% strain [19]. These two mechanisms may dynamically fluctuate between each other (inter-convert). 3) Interaction and extension of the long, flexible and partially unstructured αC region. The αC region (α221-610) consists of an unstructured connector region (α221-391), and the terminal domain (α392-610). There is evidence that interactions between the αC regions may play a role in fiber assembly, especially lateral aggregation [25-27]. It was also found that a shorter length of the αC connector (in different species) correlates with a lower extensibility of fibers [26].

This model may explain several experimental observations. 1) Two relaxation rates. If viscoelastic mechanism 1 and 2 occur at different rates and if they are inter-convertible, two different relaxation rates would be observed. For example the α-helical conversion may happen at a faster rate (and lower force) and the unfolding of the γC region may happen at a slower rate (and higher force). 2) Strain hardening occurring at about 100% strain. The faster α-helical conversion provides 100% strain, after that γ-nodule unfolding becomes dominant. 3) The dramatic and sigmoidal increase in energy loss with increasing strain. At larger strains the γ-nodule unfolds more extensively, which may not be totally reversible, thus resulting in large energy losses. 4) The elastic limit (no permanent lengthening) of uncrosslinked fibers is about

120% [11]. The α to β conversion (and initial unfolding of γ-nodule) may be largely reversible (despite some dissipative energy) and thus explain the observed 120% elastic limit of uncrosslinked fibrin fibers. 5) Brown et al. showed by force spectroscopy that a chain of fibrinogen monomers lengthens incrementally by about 90 – 100% upon the application of force [7]. The α-helical to β-strand conversion of the coiled coils is consistent with these measurements. This conversion was also observed in computational simulations [28]. 6) Stiffening and decreased elasticity of the fiber upon crosslinking. The role of the two αC regions in fiber assembly is still unclear; however, they are important for lateral aggregation [25-27]. The αC-connector region alone (α221-391) can extend 61 nm (122 nm for both), and the whole αC region (α221-610) can extend still farther. The αC region could, therefore, elastically connect fibrin monomers within a protofibril, and they can also easily reach across adjacent protofibrils. The αC region interactions may be partly responsible for the elastic recoil forces. It would explain that fully crosslinked fibers become stiffer, less elastic and less extensible. There are numerous crosslinking sites and full crosslinking may, thus, limit the mobility of the αC-connector. More insights into the role of the α–α and γ–γ crosslinks could be gained by extending our single fiber experiments to crosslinking mutants [24].

It should now be possible to use our data on the single fibers, and the data from our companion paper on the strength of fibrin fiber joints [29], to build a realistic, mechanical model of a blood clot, by utilizing recently developed network modeling approaches [6, 9, 10]. The model data could then be compared to whole clot measurements [3-5].

It would be equally interesting to build a model of a single fiber starting with an arrangement of single fibrin molecules, and testing the mechanical properties of such a model against our data.

Acknowledgments

We thank M. C. Stahle and R. R. Hantgan for help with fluorescently labeling fibrinogen, and the NIH research resource P41 EB002025 for general support. This research was supported by the NIH, R41 CA103120 (MG); NSF, CMMI-0646627 (MG); and the American Heart Association, 081503E (CRC).

Author contributions

WL, CRC, EAS and MG performed and designed research; WL, CRC and MG wrote paper

References

1 Weisel JW. The mechanical properties of fibrin for basic scientists and clinicians. *Biophysical Chemistry*. 2004; **112**: 267-76.

2 Lorand L. Acquired inhibitors of fibrin stabilization: a class of hemorrhagic disorders of diverse origins. In: Green D, ed. *Anticoagulants, Physiologic, Pathologic and Pharmacologic*. Boca Raton: CRC Press, 1994, 169-91.

3 Ryan EA, Mockros LF, Weisel JW, Lorand L. Structural Origins of Fibrin Clot Rheology. *Biophysical Journal*. 1999; **77**: 2813-26.

4 Roberts WW, Lorand LL, Mockros LF. Viscoelastic properties of fibrin clots. *Biorheology*. 1973; **10**: 29-42.

5 Benkherourou M, Gumery PY, Tranqui P. Quantification and macroscopic modeling of the nonlinear viscoelastic behavior of strained gels with varying fibrin concentrations. *Ieee Transactions on Biomedical Engineering*. 2000; **47**: 1465-75.

6 Brown AEX, Litvinov RI, Discher DE, Purohit PK, Weisel JW. Multiscale Mechanics of Fibrin Polymer: Gel Stretching with Protein Unfolding and Loss of Water. *Science*. 2009; **325**: 741-4.

7 Brown AEX, Litvinov RI, Discher DE, Weisel JW. Forced Unfolding of Coiled-Coils in Fibrinogen by Single-Molecule AFM. *Biophysical Journal*. 2007; **92**: L30 - L41.

8 Kollman JM, Pandi L, Sawaya MR, Riley M, Doolittle RF. Crystal Structure of Human Fibrinogen. *Biochemistry*. 2009; **48**: 3877-86.

9 Gardel ML, Shin JH, MacKintosh FC, Mahadevan L, Matsudaira P, Weitz DA. Elastic Behavior of Cross-Linked and Bundled Actin Networks. *Science*. 2004; **304**: 1301-5.

10 Storm C, Pastore JJ, MacKintosh FC, Lubensky TC, Janmey PA. Nonlinear elasticity in biological gels. *Nature*. 2005; **435**: 191-4.

11 Liu W, Jawerth LM, Sparks EA, Falvo MR, Hantgan RR, Superfine R, Lord ST, Guthold M. Fibrin Fibers Have Extraordinary Extensibility and Elasticity. *Science*. 2006; **313**: 634.

12 Collet JP, Shuman H, Ledger RE, Lee ST, Weisel JW. The elasticity of an individual fibrin fiber in a clot. *Proceedings of the National Academy of Sciences of the United States of America*. 2005; **102**: 9133-7.

13 Guthold M, Liu W, Stephens B, Lord ST, Hantgan RR, Erie DA, Taylor RM, Superfine R. Visualization and mechanical manipulations of individual fibrin fibers suggest that fiber cross section has fractal dimension 1.3. *Biophysical Journal*. 2004; **87**: 4226-36.

14 Carlisle CR, Coulais C, Namboothiry M, Carroll DL, Hantgan RR, Guthold M. The mechanical properties of individual, electrospun fibrinogen fibers. *Biomaterials*. 2009; **30**: 1205-13.

15 Guthold M, Falvo MR, Matthews WG, Paulson S, Washburn S, Erie D, Superfine R, Brooks FP, Taylor RM. Controlled Manipulation of Molecular Samples with the nanoManipulator. *IEEE/ASME Transactions on Mechatronics*. 2000; **5**: 189-97.

16 Sader JE, Larson I, Mulvaney P, White LR. Method for the Calibration of Atomic-Force Microscope Cantilevers. *Review of Scientific Instruments*. 1995; **66**: 3789-98.

17 Liu W, Bonin K, Guthold M. An easy and direct method for calibrating AFM lateral force measurements. *Rev Sci Instrum*. 2007; **78**: 063707.

18 Silver FH, Christiansen D, Snowhill PB, Chen Y, Landis WJ. The role of mineral in the storage of elastic energy in turkey tendons. *Biomacromolecules*. 2000; **1**: 180-5.

19 Guthold M, Liu W, Sparks EA, Jawerth LM, Peng L, Falvo M, Superfine R, Hantgan RR, Lord ST. A comparison of the mechanical and structural properties of fibrin fibers with other protein fibers. *Cell Biochemistry and Biophysics*. 2007; **49**: 165-81.

20 Litvinov RI, Gorkun OV, Owen SF, Shuman H, Weisel JW. Polymerization of fibrin: specificity, strength, and stability of knob-hole interactions studied at the single-molecule level. *Blood*. 2005; **106**: 2944-51.

21 Yang G, Cecconi C, Baase WA, Vetter IR, Breyer WA, Haack JA, Matthews BW, Dahlquist FW, Bustamante C. Solid-state synthesis and mechanical unfolding of polymers of T4 lysozyme. *PNAS*. 2000; **97**: 139-44.

22 Privalov PL, Medved LV. Domains in the Fibrinogen Molecule. *J Mol Biol*. 1982; **159**: 665-83.

23 Ryan EA, Mockros LF, Stern AM, Lorand L. Influence of a Natural and a Synthetic Inhibitor of Factor XIIIa on Fibrin Clot Rheology. *Biophysical Journal*. 1999; **77**: 2827-36.

24 Standeven KF, Carter AM, Grant PJ, Weisel JW, Chernysh I, Masova L, Lord ST, Ariens RAS. Functional analysis of fibrin gamma-chain cross-linking by activated factor XIII: determination of a cross-linking pattern that maximizes clot stiffness. *Blood*. 2007; **110**: 902-7.

25 Collet JP, Moen JL, Veklich YI, Gorkun OV, Lord ST, Montalescot G, Weisel JW. The alpha C domains of fibrinogen affect the structure of the fibrin clot, its physical properties, and its susceptibility to fibrinolysis. *Blood*. 2005; **106**: 3824-30.

26 Falvo MR, Millard D, Obrien ET, Superfine R, Lord ST. Length of tandem repeats in fibrin's alpha C region correlates with fiber extensibility. *J Thromb Haemost*. 2008; **6**: 1991-3.

27 Litvinov RI, Yakovlev S, Tsurupa G, Gorkun OV, Medved L, Weisel JW. Direct evidence for specific interactions of the fibrinogen alpha C-domains with the central E region and with each other. *Biochemistry*. 2007; **46**: 9133-42.

28 Lim BBC, Lee EH, Sotomayor M, Schulten K. Molecular basis of fibrin clot elasticity. *Structure*. 2008; **16**: 449-59.

29 Carlisle CR, Sparks EA, Der Loughian C, Guthold M. Strength and Failure of Fibrin Fiber Branch Points. *Journal of Thrombosis and Haemostasis (co-submitted)*. 2009.

Tables

Fiber Type	Crosslinked	Uncrosslinked
ε_{max}	147 % +/- 5%	226% +/- 8.7%*
$\varepsilon_{elastic}$	< 50 %	120 % *
E_0 (MPa)	8.0 +/- 1.0	3.9 +/- 0.6
E_∞ (MPa)	4.0 +/- 0.6	1.9+/- 0.3
τ_1 (s)	2.1 +/- 0.2	3.6+/- 1.3
τ_2 (s)	49 +/- 4	57 +/- 8
h	1.9 +/- 0.3	3.0 +/- 0.3
E_{loss}	0-70%	≤40-70%

Table 1. Mechanical properties of fibrin fibers; the average values and standard errors are listed; see supplement for partially crosslinked fibers and statistics). Extensibility, ε_{max}; elastic limit, $\varepsilon_{elastic}$; E_0, total elastic modulus; E_∞ relaxed elastic modulus; τ_1 fast relaxation time; τ_2 slow relaxation time; h, strain hardening factor (ratio of the total modulus at low strains (0-80%) to the total modulus at high strains (above 110%). Thus, the total elastic modulus for uncrosslinked fibers has a value of 3.9 MPa at low strains and 11.7 MPa at high strains. Crosslinked fibers did not show consistent strain hardening. E_{loss}, percent energy loss per stretch cycle (energy loss at low strains is close to 0% for uncrosslinked, and ≤40% for crosslinked fibers).

* Values from [11].

Figure Legends

Figure 1. Experimental set-up. (A) Schematic of AFM sitting on top of the inverted optical microscope. **(B)** Top view of stretched fiber. The initial and stretched states are in dotted gray and solid black, respectively. **(C)** Typical fibrin fiber stress-strain curve. **(D-F)** Fluorescence microscopy movie frames of a stretching experiment. The fiber is anchored on two ridges (brighter, horizontal, 8 μm wide bars) and suspended over a groove (darker, horizontal, 12 μm wide bars); the AFM cantilever appears as a 35 μm wide, dark rectangle; the AFM tip is indicated as a green dot.

Figure 2. Strain hardening. (A) Stress-strain curve of an uncrosslinked fibrin fiber. **(B)** The total elastic modulus, E_0, (slope of forward curve in **(A)**) as a function of strain. **(C)** Stress-strain curve for a crosslinked fibrin fiber.

Figure 3. Energy loss. A) Stress-strain curve for three consecutive pulls of uncrosslinked fiber with strains of 48%, 85% and 125%. The energy loss corresponds to the area inscribed in a cyclical stress-strain curve. **B)** Ratio (percentage) of energy lost vs. total energy for crosslinked fibers (green) and uncrosslinked fibers (blue). Sigmoidal fitting curves of the form

$R = R_1 + \frac{R_2 - R_1}{1 + e^{-\frac{\varepsilon - \varepsilon_0}{s}}}$, were used to fit the data. R_1 is the initial value, R_2 is the final value, ε_0 is the strain at the inflection point.

Figure 4. Incremental stress-strain curves. (A) Strain vs. time and **(B)** stress vs. time for an incremental stress-strain curve of a fibrin fiber. The x-axis (time) is the same for **(A)** and **(B)**. The strain is held constant at 23%, 46%, 75%, 104%, and 138% for about 120 seconds. The stress decays exponentially at each strain value. **(C)** Total stress (red curve, squares) and relaxed stress (blue curve, dots) vs. strain as obtained from the data in **(A)** and **(B)**.

Figure 5. Model for fibrin fiber extensions. (A) Crystal structure of fibrinogen[8]; the Aα chains, Bβ chains and γ chains are in blue, red and green, respectively. A cartoon depiction of the flexible αC region is added to the crystal structure as a blue line and blue square, αC regions may interact with each other within a protofibril, and across protofibrils. **(B)** Schematic model of half-staggered assembly of three fibrin monomers into protofibril, (β–nodule is no longer depicted). **(C)** An α-helix to β-strand conversion of the coiled coil and a slight straightening and alignment of the molecules could accommodate ~100% strain. Some of the αC regions are also extended at this point. **(D)** Higher strains, up to 320% could be accommodated by a partial unfolding of the globular γ-nodule; 230% strain is depicted. Further extension of the αC region

could occur. **(E)** Interactions between αC regions promote lateral aggregation of protofibrils; they can be elastically extended.

Supplement

The mechanical properties of single fibrin fibers

W. Liu[1], C. R. Carlisle[1], E. A. Sparks[1], M. Guthold[1†]

[1]Dept. of Physics, 7507 Reynolda Station, Wake Forest University, Winston-Salem, NC 27109
W. Liu and C. R. Carlisle contributed equally to this manuscript

The supplement contains the following sections:

---

1. Materials and Methods

***Preparation of Oregon-Green-labeled fibrinogen*.** Factor XIII-free fibrinogen (American Diagnostica, Inc. Greenwich, CT) was fluorescently labeled with about two Oregon Green 488 (OG) molecules as reported previously [1].

Preparation of striated substrate. The striated substrate was prepared as reported previously [1]. It was obtained by pressing a PDMS (polydimethylsiloxane) stamp into a 10 µl drop of Norland Optical Adhesive-81 (NOA-81; Norland Products, Inc. Cranbury, NJ) on a clean, 60 mm x 22 mm, # 1.5 microscope cover slip (Fisher Scientific, Pittsburgh, PA). The NOA-81 was cured

with UV light (365 nm) (UVP 3UV transilluminator, Upland CA) for about 70 seconds and the PDMS stamp was removed.

Fibrin fiber formation. Fibrin fibers were formed as reported previously [1]. To form uncrosslinked fibrin fibers, OG-labeled fibrinogen was diluted in "fibrin buffer" (140 mM NaCl, 10 mM Hepes, 5 mM $CaCl_2$, pH 7.4); final concentration, 0.5 mg/ml. 18 μl of the fibrinogen solution were deposited onto the striated substrate and 2 μl of thrombin (final concentration: ~ 0.1 NIH unit/ml, Enzyme Research Lab, South Bend, IN) were mixed in to start fiber formation. After incubation for 1 hr in a saturated atmosphere, the sample was rinsed with and stored in fibrin buffer. To form crosslinked fibers, fibrinogen (American Diagnostica Inc, CT; final concentration 1 mg/ml) and Factor XIII (Enzyme Research Labs, South Bend, IN; final concentration, 25 Loewy units/ml) was combined before adding thrombin. A different fluorescence labeling method was used for crosslinked fibers. The fibers were labeled after formation through incubation for 10 minutes in calcium free fibrin buffer with carboxylate modified, 20 nm, yellow-green FluoSpheres (Molecular Probes, Invitrogen, USA).

Combined AFM/fluorescence microscopy. The mechanical manipulations on fibrin fibers were performed with a combined atomic force microscope/optical microscope instrument. The schematic set-up is shown in Figure 1 (main manuscript) and a more detailed description is given in [1, 2]. The instrument is based on an inverted Zeiss Axiovert 200 microscope (Zeiss, Thornwood NY), a Hamamatsu EM-CCD C9100 Camera (Hamamatsu Photonics KK, Japan), IPLab software (Scanalytics, Fairfax, VA) and a Topometrix Explorer AFM (Veeco Instruments, Woodbury, NY). The microscope stage was designed so that the AFM tip, fiber sample and objective lens can move with respect to each other, which allows alignment of the fiber with the AFM tip and objective lens. We used NT-MDT CSCS12 and NSC12 silicon cantilevers with a rectangular cross-section (Mikromasch, Wilsonville, OR).

Manipulating fibrin fibers. The AFM manipulation experiments were done with a nanoManipulator (3^{rd} Tech, Chapel Hill, NC), a software program that interfaces the AFM with a force feedback stylus (PHANTOM, Sensable Technologies, Woburn, MA) and a graphics computer [3]. The nanoManipulator provides control over the x-, y- and z-movement of the AFM tip. For these experiments, the AFM tip was held at a constant height, so that the apex of the AFM tip was about 1 μm under the fiber. As illustrated in Fig. 1, the tip of the atomic force microscope (AFM) is then moved laterally to stretch fibers that are suspended across channels on

the striated substrate. The initial fiber length, L_{init}, was determined from optical images; the stretching displacement, s, was determined via AFM; the fiber strain $\varepsilon = (L'-L_{init})/L_{init}\cdot 100\%$ was determined using trigonometry ($L'^2 = s^2 + L_{init}^2$).

Determination of the stress involved several steps. The measured quantity is the "left – right" photocurrent of the AFM photodiode, I_l, which results from the deflection of the cantilever. This signal needs to be converted into force, F. We typically used the Sader method [4], based on cantilever geometry and resonance frequency (outlined below) and verified it with the Liu method, based on bending a glass fiber[5]. For rectangular cantilevers,

$F_l = \frac{Ewt^3}{6L^2(h+t/2)} \cdot S_n \cdot I_l$ (see [5]), where $E = 1.69\cdot 10^{11}$ N/m^2 is the Young's modulus of the cantilever material (silicon), w, t and L are the width, thickness and length of the cantilever and h is the tip height. $S_n = \Delta z/\Delta I_n$ is the sensitivity, where Δz is normal (height) displacement of the cantilever and I_n is the top – bottom photocurrent. We measured the cantilever length and width and tip height with the inverted optical microscope. The thickness of the cantilever was determined from $f_0 = \frac{1.02t}{2\pi L^2\sqrt{E/\rho}}$, where f_0 is the resonance frequency of the cantilever and ρ = 2330 kg/m^3 is the density of the silicon. The force applied to the fiber was then determined at each strain using the lateral force applied to the cantilever tip in conjuction with balancing of forces between the cantilever and the two halves of the fibers $F = \frac{F_l}{2\cdot\sin\alpha}$, where α is the angle between the initial position of the fiber and the current position, see Fig. 1 B (main manuscript). The diameter of each fiber was determined by AFM-imaging the fiber near the anchoring points on top of the ridges. Stress is calculated via $\sigma = F/A$, where F is force and A is the *initial* fiber cross-section (we assumed a circular fiber cross-section).

Estimation of instrumentation error. We estimate that the errors in the force calibration, fiber diameter determination by AFM, and the strain determination by optical microscopy and AFM are about 30%, 20% and 5%, respectively.

Strain hardening. Fig. 2B (main text) shows the *slope* of Fig. 2A (main text). Fig. 2B was obtained by determining $\Delta\sigma/\Delta\varepsilon$ for each data point of the stress-strain curve shown in a window of $\Delta\varepsilon = 20\%$.

Energy loss: (Fig. 3, main text)). The graph contains 24 and 61 data points for uncrosslinked and crosslinked fibers respectively. The data were smoothed by taking the sliding average of an ε = 30% window with an ε = 15% step size.

SDS Protein Gel Electrophoresis: Fibrin samples for manipulation were prepared in parallel with samples to be used for protein gel analysis of fibrin crosslinking. Just like the samples prepared for manipulation, the samples for gel analysis were allowed to clot for 1 hr before adding reducing buffer and sampling buffer (Bio-Rad Lab Inc, Hercules, CA). The tubes were heated at 100ºC for 10 minutes and stored at -80ºC until the gel was run. Polyacrylamide protein gel, 4% stacking and 7.5% resolving, electrophoresis in SDS was used for molecular weight separation and the proteins were stained with commassie blue staining. Crosslinking was determined through density comparison of the beta to gamma band ratio or beta to alpha band ratio of uncrosslinked samples to partially crosslinked or crosslinked samples.

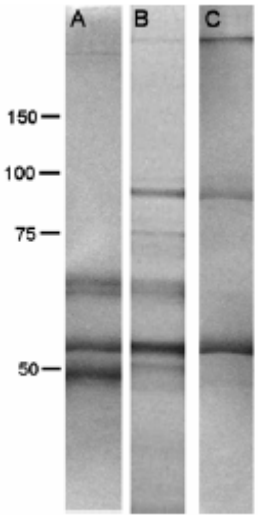

Figure S1. SDS Protein Gel. (A) Lane of an uncrosslinked fibrin sample. The three bands from top to bottom are the alpha, beta and gamma chains of the fibrin monomers. **(B)** Partially crosslinked fibrin lane. The beta chain does not crosslink and therefore remains dark, while the alpha and gamma bands become lighter. A band consistent with gamma-gamma crosslinking appears around 98 kDa. **(C)** Fully crosslinked fibrin lane. The alpha and gamma bands have disappeared and gamma-gamma and alpha multimer bands appear at higher molecular weights. The alpha multimers appear at the top of the gel.

2. Additional d Information on Fibrin Fiber Mechanical Properties

2.1 Elastic modulus vs. radius. The average diameter of the crosslinked fibers was 390 nm, with a range of 124 nm to 800nm. The average diameter of noncrosslinked fibers was 180 nm, with a range of 94 nm to 708 nm. A plot of the total elastic modulus E_0 versus diameter, showed a trend of decreasing modulus with increasing diameter (Fig. S2). A similar trend was observed for the rupture force dependence of dry fibrin fibers on diameter [2]. This suggests that the core of fibrin

fibers is denser than the periphery. The decreasing modulus can be fit with a power law of the form $E_o = cr^n$ where r is the radius of the fiber. For crosslinked and uncrosslinked fibers fibrin fibers r is -1.7 and -0.89, respectively (slope of log-log plot in Figure S2).

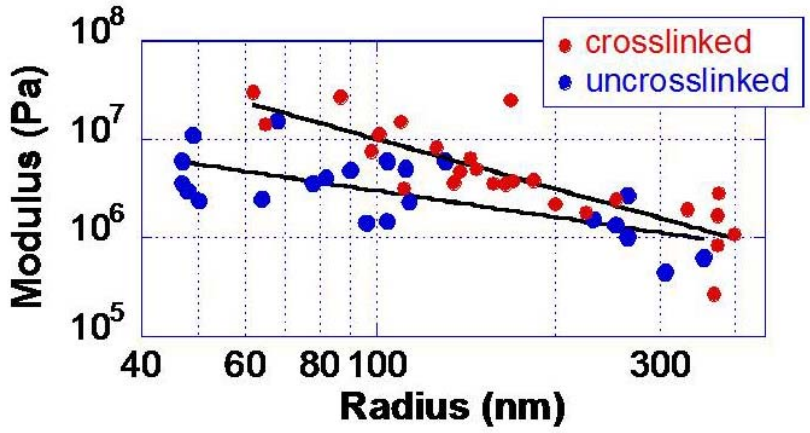

Figure S2 Log-log plot of the total elastic modulus for crosslinked fibrin fibers vs. radius of the fiber. Modulus values decrease as fiber radius increases. The data were fit by a power law; $E_o = cr^n$ where r is the radius of the fiber and n = -1.7 and -0.89 for crosslinked and uncrosslinked fibers, respectively.

2.2 Stress relaxation and generalized Kelvin model. Stress relaxation in incremental stress-strain curves is indicative of viscous (time-dependent) processes [6], and may be fitted by exponentials of the form

$$\sigma(t) = \sigma_\infty + \sum_i \sigma_i \cdot e^{-t/\tau_i} \qquad (1).$$

Mechanistically this implies that upon stretching, elastic and viscous molecular processes occur within the fibrin fiber. In our model in Fig. 5 (main manuscript), we propose three different molecular mechanisms. $\sigma(t)$ is the stress at any time t after relaxation started, σ_i is the stress due to time-dependent elements (see Kelvin model below), τ_i is the relaxation time and σ_∞ is the stress left in the fully relaxed fiber ($t \rightarrow \infty$). We have analyzed the relaxation processes of fibrin fibers at different strains. Figure S3A shows a typical stress relaxation curve for a fibrin fiber (red curve). Initially, stress relaxation is dominated by a fast relaxation rate, then by a slower rate. A fitting curve, with two relaxation times, τ_1= 1.3 s and τ_2= 22.9 s, is applied in Figure S3A

(green line); it matches the data in the fast and slow relaxation regions very well. Using only a single relaxation time did not suffice to fit the data (blue line); it could only match either the slow or the fast relaxation region. Crosslinked partially crosslinked and uncrosslinked fibers required a minimum of two stress-relaxation rates for accurate fitting. As listed in Table S1, all have nearly the same fast rate (2 s to 4 s) and slow rate (49 s to 57 s). In Figure S3B, the relaxation rates are plotted as a function of strain and, although there is significant scatter, it appears that the relaxation times are independent of strain.

A simple mechanical model that can account for these observations (the two relaxation rates; stress does not decay to zero) is a generalized Kelvin model, consisting of an elastic spring with modulus E_∞, in parallel with two Maxwell elements consisting of a dashpot and a spring in series (Figure 3C). For this model, the equation for stress relaxation becomes

$$\sigma(t) = \varepsilon_0\left[E_\infty + E_1 \cdot e^{-t/\tau_1} + E_2 \cdot e^{-t/\tau_2}\right] \qquad (2).$$

E_∞ is the relaxed elastic modulus, E_0 is the total elastic modulus, $E_0 = E_\infty + E_1 + E_2$. The relaxation times, the elastic modulus of the springs, and the viscosity of the dashpot elements are related via $\tau_1 = \mu_1/E_1$ and $\tau_2 = \mu_2/E_2$. As described above, we have measured E_∞, E_0, τ_1, τ_2, which are model-independent. Fitting the data to the generalized Kelvin model we have determined E_1, E_2, μ_1, and μ_2, which are model-dependent (see table S1).

The Kelvin model is intended as a macroscopic model that behaves mechanically equivalently to the fibers. Although the Kelvin model elements may not necessarily correspond to actual physical fiber elements, it is intriguing, and tempting to speculate that the Kelvin model elements may correspond to the three elements of our molecular model (Fig. 5, main text): 1) α-helix to β-strand conversion of the two coiled coils of the fibrin monomer. 2) Deformation or partial unfolding of the γ-nodule of the fibrin monomer. 3) Interaction and extension of the long, flexible and partially unstructured αC region.

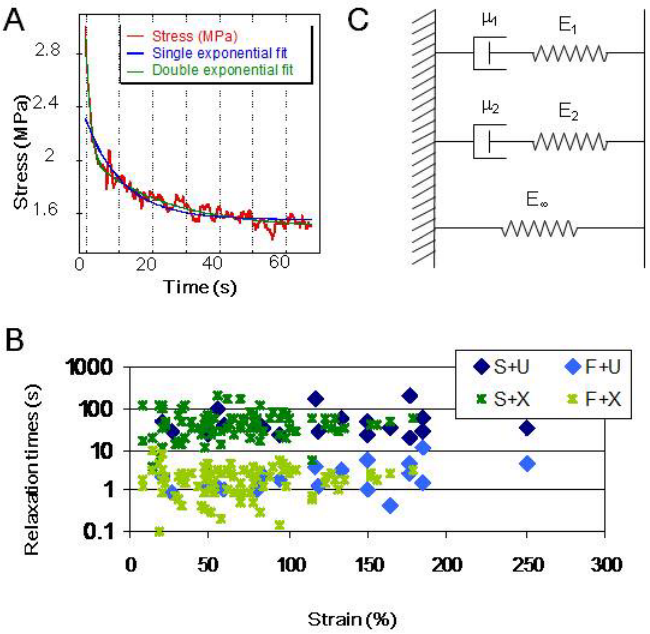

Figure S3. Stress relaxation and generalized Kelvin model. (A) A fibrin fiber stress relaxation curve (red) fitted with a single exponential relaxation curve, $\sigma_0(t) = \sigma_1 \cdot e^{-t/\tau_1} + \sigma_\infty$ (blue), and a double exponential relaxation curve, $\sigma_0(t) = \sigma_1 \cdot e^{-t/\tau_1} + \sigma_2 \cdot e^{-t/\tau_2} + \sigma_\infty$ (green), where τ_i are the relaxation times and σ_0 is the fully relaxed elastic stress. Pearson's R value for the single relaxation fit is 0.91 and 0.98 for the double relaxation fit. The fitting coefficient for the double relaxation are τ_1 = 1.3 s, τ_2 = 22.9 s and σ_0 = 2.2MPa. **(B)** Fast (F) and slow (S) relaxation times as a function of strain for crosslinked (X), uncrosslinked fibers (U). **(C)** Generalized Kelvin model consisting of a spring (elastic modulus E_∞), in parallel with two Maxwell elements (each consisting of a dashpot (viscosity η_1, η_2; relaxation time τ_1, τ_2) in series with a spring (elastic modulus E_1, E_2).

2.3. Detailed force per monomer and energy per monomer calculations. The force and energy *per fibrin monomer* can also be estimated from our data and compared with single protein unfolding experiments and melting experiments. For example, the fibrin fiber in Figure 2 contains about 1600 monomers per cross-section (fiber radius, 165 nm; fibrin monomer radius, 2.25 nm; 30% protein content of fiber [7]) and a force of 220 nN is required to stretch it to 100% strain. Thus, the force per monomer at 100% strain is about 140 pN, which is consistent with the 100 pN force to stretch a single fibrin monomer by 100% found by Brown et al. [8]. Using similar considerations, we estimate the rupture force per monomer to be about 280 pN (ε_{max}=147%, strain hardening h=1.9). This value is similar to the 260 pN (2·130 pN) required to

rupture the two A:a interactions between half-staggered monomers within a protofibril [9]. For comparison, the unfolding forces of T4 lysozyme (mainly α-helical) and the titin Ig-domain (mainly β-structure) are 64 pN [10] and 150-300 pN [11], respectively. Thus, judging by these force considerations, it is certainly possible that some regions of the fibrin monomer unfold *before* the fiber ruptures.

The energy required to rupture the fiber is of the same order of magnitude as the melting enthalpy of the fibrin molecules contained in the fiber. Again, using Figure 2, the energy to rupture the fiber (area under curve) is approximately $8 \cdot 10^{-13}$ J. Assuming that there are about 570,000 monomers in this fiber (fiber length and radius, 15,200 nm and 165 nm; fibrin monomer length and radius, 45 nm and 2.25 nm; 30% protein content of fiber), the rupture energy per monomer is about $4 \cdot 10^{-17}$ J ($2.4 \cdot 10^{3}$ kJ/mol). When taking melting curves of fibrinogen, two major peaks are observed [12]. The low-temperature peak (56°C) likely corresponds to three separate melting events within the D region and the high-temperature (95°C) peak likely corresponds to a melting event within the E region and the melting of the coiled coils. The enthalpy of melting (area under curve) of the low-temperature peak is 3350 kJ/mol and of the high temperature peak 1300 kJ/mol. The total enthalpy of melting (4650 kJ/mol) is, thus, of the same order of magnitude as the rupture energy (2400 kJ/mole), again indicating that fibrin may melt (denature), before the fiber ruptures.

2.4 Mullins Effect. Our data were all collected from 'first pulls' or 'small pulls'; that is from fibers that had not been significantly stretched before. The "Mullins effect" refers to the phenomenon that the force required to stretch a polymer is smaller in the second loading cycle then it was in the first cycle. This effect has been observed in a number of materials such as rubber, filler-reinforced vulcanized rubber, rubber-like materials, and rat left ventricular myocardium tissue [13]. We observed a Mullins effect in fibrin fibers when the strain is over 30%, 100% and 60% for crosslinked, partially crosslinked (see supplement) and uncrosslinked fiber, respectively. Figure S4 shows consecutive stress-strain curves of a fiber that was stretched to the same strain three times. The loading curve for the second pull (purple curve) is significantly smaller than for the first pull (red curve), although the unloading curves are very similar for these two. For the third pull (green curve) and all the following pulls (if fiber is not stretched even farther), the loading and unloading curve will follow almost the same path as the second pull.

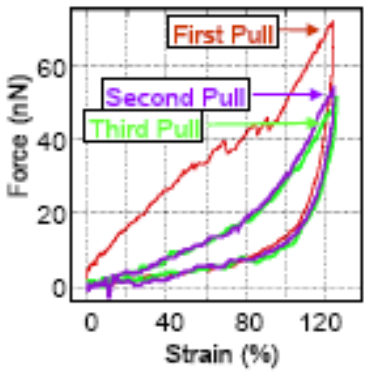

Figure S4. Mullins effect. Three consecutive loading cycles of 120% strain were applied to same fibrin fiber. The forward force for the first pull is larger than for the second and third pull. The forward forces for the second and third cycle overlap and all return paths nearly overlap.

3. Partially Crosslinked Fibrin Fibers.

Partially crosslinked fibers were formed as previously reported [1]. Factor XIII (Enzyme Research Labs, South Bend, IN; final concentration, 100 Loewy units/ml) was added to the fibrinogen and buffer solution before thrombin was added. Other conditions and concentrations were the same as those used to form uncrosslinked fibers. SDS gel electrophoresis of the partially crosslinked samples showed 50 – 75% γ–γ crosslinking and 25 – 60% α–α crosslinking (Fig S1). We don't completely understand why these fibers did not fully crosslink. Nevertheless, we feel that the results on the partially crosslinked fibers should be communicated for at least two reasons. First, they may be physiologically relevant as they represent an intermediate state between uncrosslinked and fully crosslinked fibers. Second, they show extraordinary mechanical properties. As previously reported, partially crosslinked fibers have an extensibility of 333% and an elastic limit of 180%, both values higher than those for uncrosslinked and crosslinked fibrin fibers [1]. Partial crosslinking increased the extensibility and elastic limit, while the stiffness only slightly increased and the strain hardening and energy loss behavior remained similar to that of uncrosslinked fibers. We speculate that the more fully formed γ–γ crosslinks are responsible for the large extensibility, as these crosslinks may stabilize the fiber in the longitudinal direction.

Partially crosslinked fiber viscoelastic properties. Identical experiments to the ones reported in the main paper were done for partially crosslinked fibers. The results are summarized in table S1. Engineering stress and incremental stress-strain curves were used to determine the total elastic modulus (4.6 MPa), the relaxed elastic modulus (2.6 Mpa) and the relaxation times (2s and 54s)

of the partially crosslinked fibers. The generalized Kelvin model was once again used to fit the relaxation, such that elastic moduli of the springs, E_1 and E_2, and viscosities of the dashpot elements, μ_1 and μ_2, were determined. Partially crosslinked fibers showed similar strain hardening, $h = 3.5$ ($p \leq 0.0015$), and energy loss characteristics to uncrosslinked fibers. Energy loss increases sigmoidally, with a low energy loss at strains below 50% which then increases to a higher total energy loss at strains above 100%. Although energy loss increases as strain increases, as previously reported, partially crosslinked fibers can be strained up to about $\varepsilon = 180\%$ and still visibly return to their initial length [1].

In our partially crosslinked fibers, γ–γ crosslinks were predominant. While in the crosslinked fibers γ–γ and α–α crosslinking was complete (within the detection limit of the SDS PAGE) . Our data suggest that the fully formed α–α crosslinks may be largely responsible for not only reducing fiber extensibility but also stiffening the fiber. Physiologically, γ–γ crosslinks form more rapidly than α–α crosslinks [14]. Therefore, the properties of partially crosslinked fibers may be representative of fibers found in newly forming clots which then progress with time to fully crosslinked fiber properties.

4. Table S1. All mechanical properties of uncrosslinked, crosslinked, and partially crosslinked fibrin fibers; including generalized Kelvin model properties, and data statistics.

Fiber Type	Crosslinked	Partially Crosslinked	Uncrosslinked
ε_{max}	147 % +/- 5%	333 % +/- 13%*	226% +/- 8.7%*
$\varepsilon_{elastic}$	< 50 %	180 % *	120 % *
E_0 (Mpa)	8.0 +/- 1.0	4.6 +/- 0.7	3.9 +/- 0.3
E_∞ (Mpa)	4.0 +/- 0.6	2.6 +/- 0.3	2.0 +/- 0.2
τ_1 (s)	2.1 +/- 0.2	2.0 +/- 0.2	2.9 +/- 0.5
τ_2 (s)	49 +/- 4	54 +/- 7	54 +/- 9
h	1.9 +/- 0.3	3.5 +/- 0.8	3.2 +/- 0.4
E_{loss}	0-70%	0-70%	≤40-70%
E_1 (Mpa)	1.3 +/- 0.2	1.1 +/- 0.3	1.6 +/- 0.8
E_2 (Mpa)	2.0 +/- 0.2	0.8 +/- 0.12	0.6 +/- 0.2
μ_1 (Mpa*s)	3.2 +/- 0.6	1.0 +/- 0.4	2.5 +/- 0.6
μ_2 (Mpa*s)	155 +/- 47	33 +/- 6.9	37 +/- 17

Table S1. Summary of mechanical properties of single fibrin fibers. The average values and standard errors are listed. Extensibility, ε_{max}, (89 data points, crosslinked fibers), elastic limit, $\varepsilon_{elastic}$, (55 data points, crosslinked fibers), E_0, total elastic modulus; E_∞ relaxed elastic modulus (moduli obtained from 86 crosslinked and 38 uncrosslinked data points collected over the entire strain range). τ_1 fast relaxation time; τ_2 slow relaxation time (average values of 86 data points for crosslinked fibers and 71 data points for uncrosslinked fibers). h, strain hardening factor; this is the ratio of the total modulus at low strains (0-80%) to the total modulus at high strains (above 110%) (average values of 26 uncrosslinked fibers). Thus, the total elastic modulus for uncrosslinked fibers has a value of 3.9 MPa at low strains and 11.7 MPa at high strains. Crosslinked fibers did not show consistent strain hardening. E_{loss}, energy loss at high strains (energy loss at low strains is close to 0% for uncrosslinked, and ≤40% for crosslinked fibers). ε_{max}, $\varepsilon_{elastic}$, E_0, E_∞, τ_1, τ_2, h, are measured values; E_1, E_2, μ_1, μ_2 are model-based values obtained by fitting our relaxation data to the generalized Kelvin model depicted in Figure S3C.
* Values were obtained from [1].

5. Movie Supplement

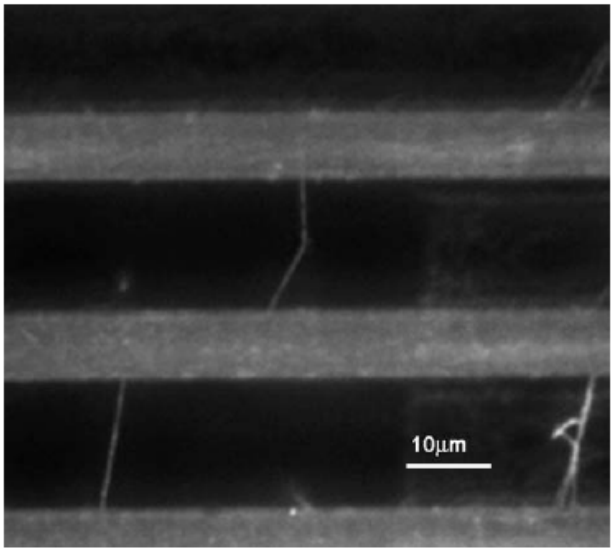

Movie 1. Crosslinked Fibrin Movie. A crosslinked fibrin fiber is first stretched and released showing visible deformation to the fiber. Next the fiber is stretched until it ruptures. The shadow of the AFM cantilever is visible above the fiber. The 8 μm wide horizontal ridges of the striated substrate are light, while the 12 μm wide grooves are dark.

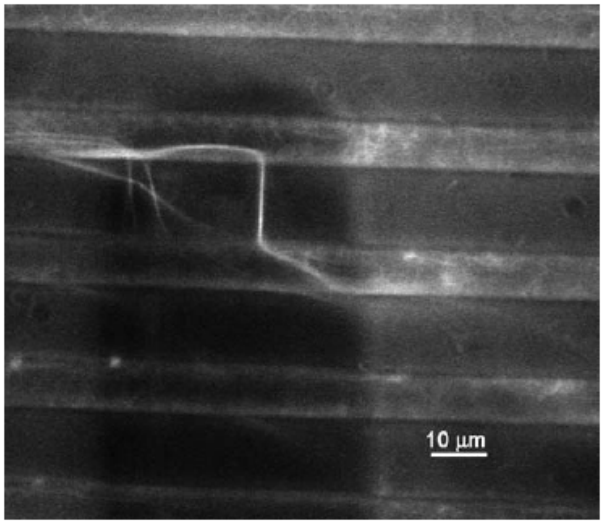

Movie 2. Uncrosslinked Fibrin Movie. An uncrosslinked fibrin fiber is stretched and returned to its initial position multiple times before being stretched until rupture. The uncrosslinked fiber undergoes significant strain without showing visible signs of deformation. The shadow of the AFM cantilever can be seen above the fiber while the 8 μm wide ridges and 12 μm wide grooves of the striated substrate are also visible as light and dark bands, respectively.

6. References

1 Liu W, Jawerth LM, Sparks EA, Falvo MR, Hantgan RR, Superfine R, Lord ST, Guthold M. Fibrin Fibers Have Extraordinary Extensibility and Elasticity. *Science*. 2006; **313**: 634.

2 Guthold M, Liu W, Stephens B, Lord ST, Hantgan RR, Erie DA, Taylor RM, Superfine R. Visualization and mechanical manipulations of individual fibrin fibers suggest that fiber cross section has fractal dimension 1.3. *Biophysical Journal*. 2004; **87**: 4226-36.

3 Guthold M, Falvo MR, Matthews WG, Paulson S, Washburn S, Erie D, Superfine R, Brooks FP, Taylor RM. Controlled Manipulation of Molecular Samples with the nanoManipulator. *IEEE/ASME Transactions on Mechatronics*. 2000; **5**: 189-97.

4 Sader JE, Green CP. In-plane deformation of cantilever plates with applications to lateral force microscopy. *Review of Scientific Instruments*. 2004; **75**: 878-83.

5 Liu W, Bonin K, Guthold M. An easy and direct method for calibrating AFM lateral force measurements. *Rev Sci Instrum*. 2007; **78**: 063707.

6 Benkherourou M, Gumery PY, Tranqui P. Quantification and macroscopic modeling of the nonlinear viscoelastic behavior of strained gels with varying fibrin concentrations. *Ieee Transactions on Biomedical Engineering*. 2000; **47**: 1465-75.

7 Carr ME, Hermans J. Size and Density of Fibrin Fibers from Turbidity. *Macromolecules*. 1978; **11**: 46-50.

8 Brown AEX, Litvinov RI, Discher DE, Weisel JW. Forced Unfolding of Coiled-Coils in Fibrinogen by Single-Molecule AFM. *Biophysical Journal*. 2007; **92**: L30 - L41.

9 Litvinov RI, Gorkun OV, Owen SF, Shuman H, Weisel JW. Polymerization of fibrin: specificity, strength, and stability of knob-hole interactions studied at the single-molecule level. *Blood*. 2005; **106**: 2944-51.

10 Yang G, Cecconi C, Baase WA, Vetter IR, Breyer WA, Haack JA, Matthews BW, Dahlquist FW, Bustamante C. Solid-state synthesis and mechanical unfolding of polymers of T4 lysozyme. *PNAS*. 2000; **97**: 139-44.

11 Rief M, Gautel M, Oesterhelt F, Fernandez JM, Gaub HE. Reversible unfolding of individual titin immunoglobulin domains by AFM. *Science*. 1997; **276**: 1109-12.

12 Privalov PL, Medved LV. Domains in the Fibrinogen Molecule. *J Mol Biol*. 1982; **159**: 665-83.

13 Johnson MA, Beatty MF. A Constitutive Equation for the Mullins Effect in Stress Controlled Uniaxial Extension Experiments. *Continuum Mechanics and Thermodynamics*. 1993; **5**: 301-18.

14 McKee PA, Mattock P, Hill RL. Subunit Structure of Human Fibrinogen, Soluble Fibrin, and Cross-Linked Insoluble Fibrin. *PNAS*. 1970; **66**: 738-44.

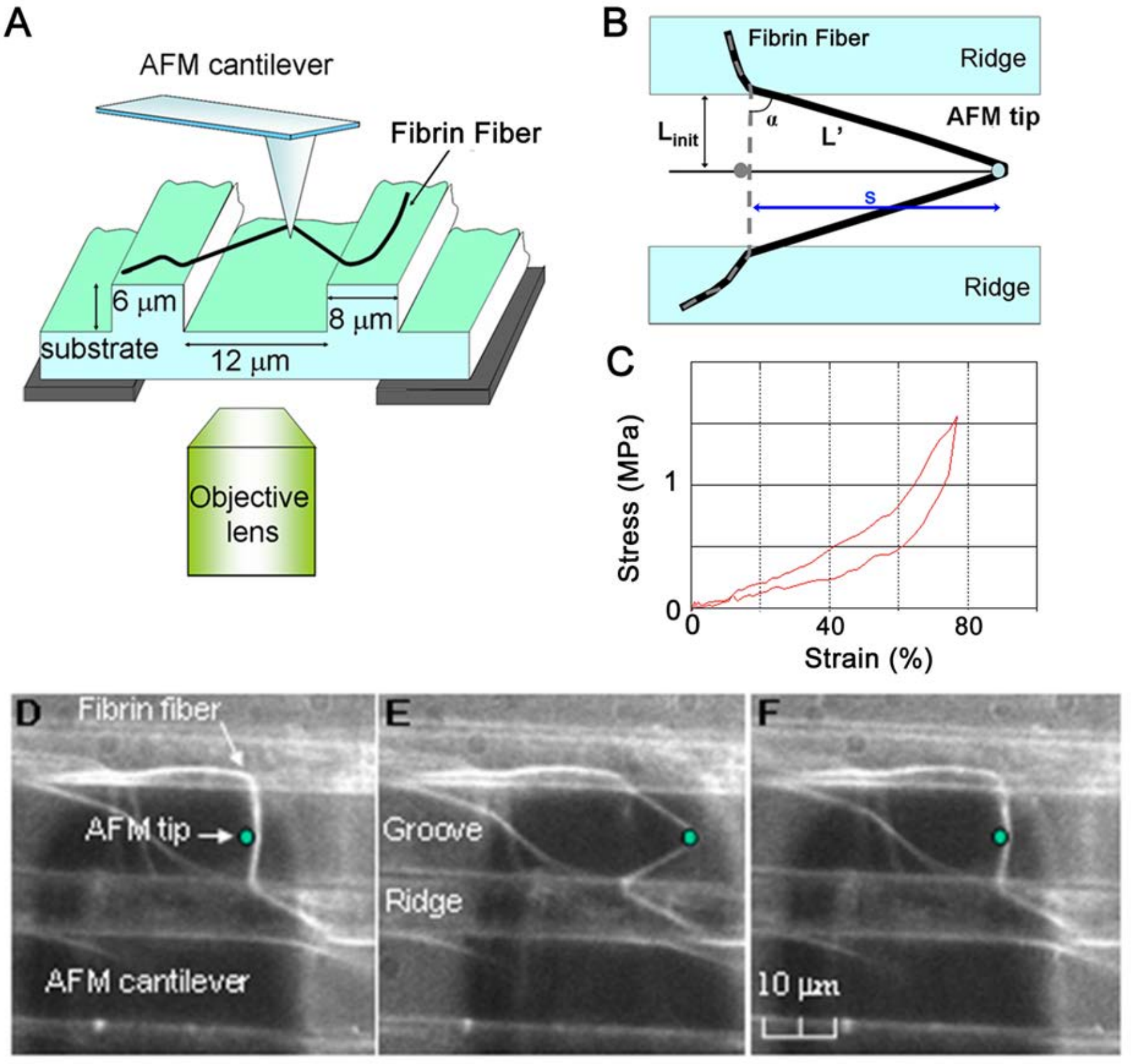
A
AFM cantilever
Fibrin Fiber
6 μm
8 μm
substrate
12 μm
Objective lens
B
Fibrin Fiber
Ridge
AFM tip
α
L'
L init
s
Ridge
C
Stress (MPa)
1
0
0
40
80
Strain (%)
D
Fibrin fiber
AFM tip
AFM cantilever
E
Groove
Ridge
F
10 μm

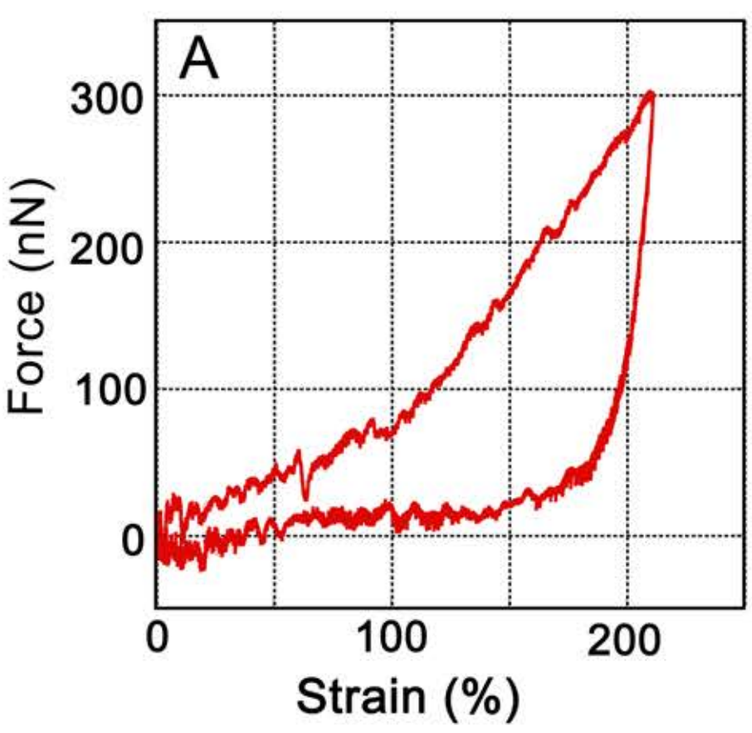
A
300
200
100
0
Force (nN)
0
100
200
Strain (%)

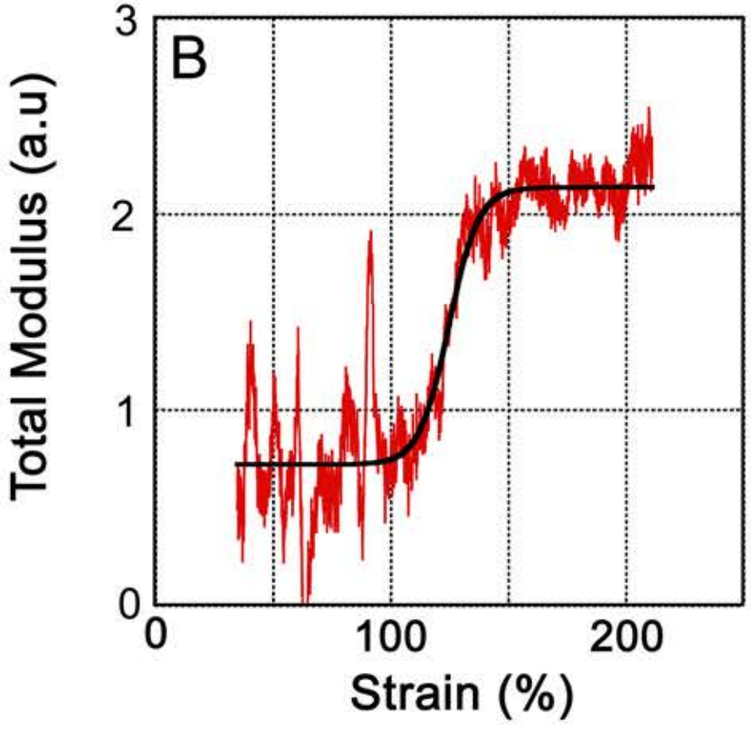
B
3
2
1
0
Total Modulus (a.u)
0
100
200
Strain (%)

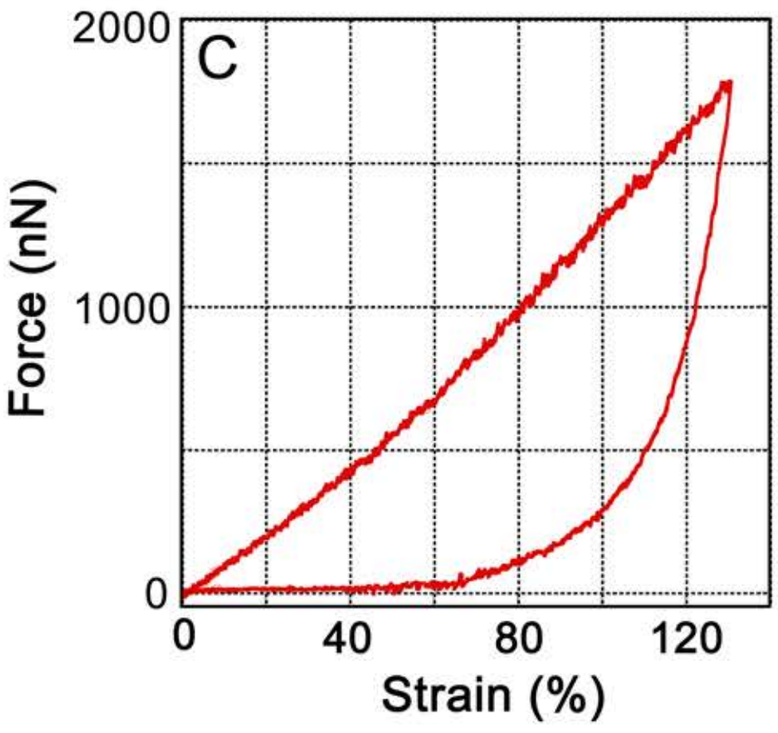
C
2000
1000
0
Force (nN)
0
40
80
120
Strain (%)

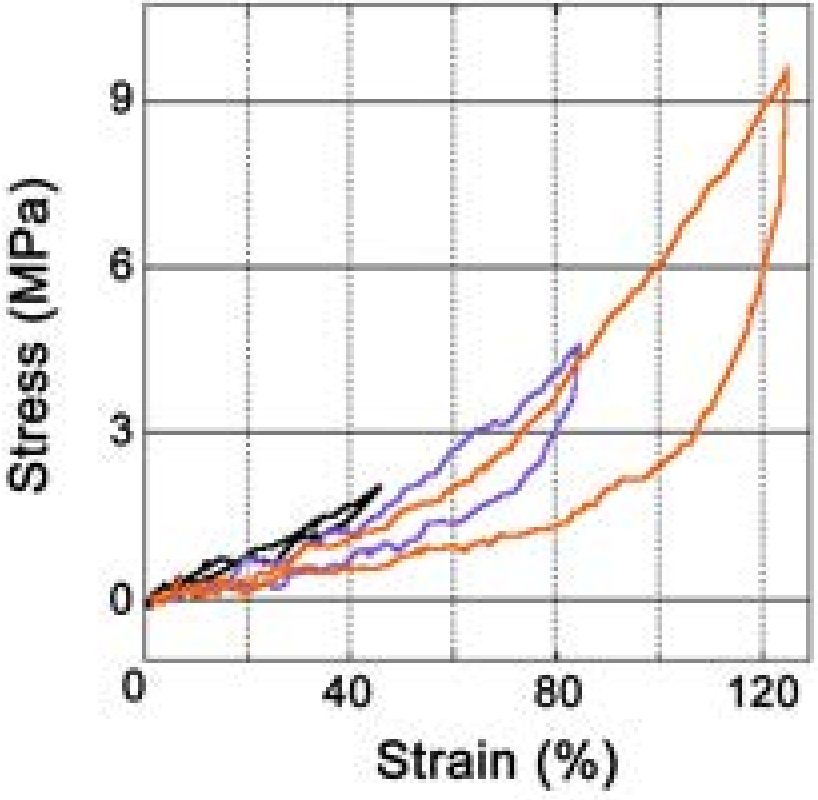
Stress (MPa)
9
6
3
0
0
40
80
120
Strain (%)

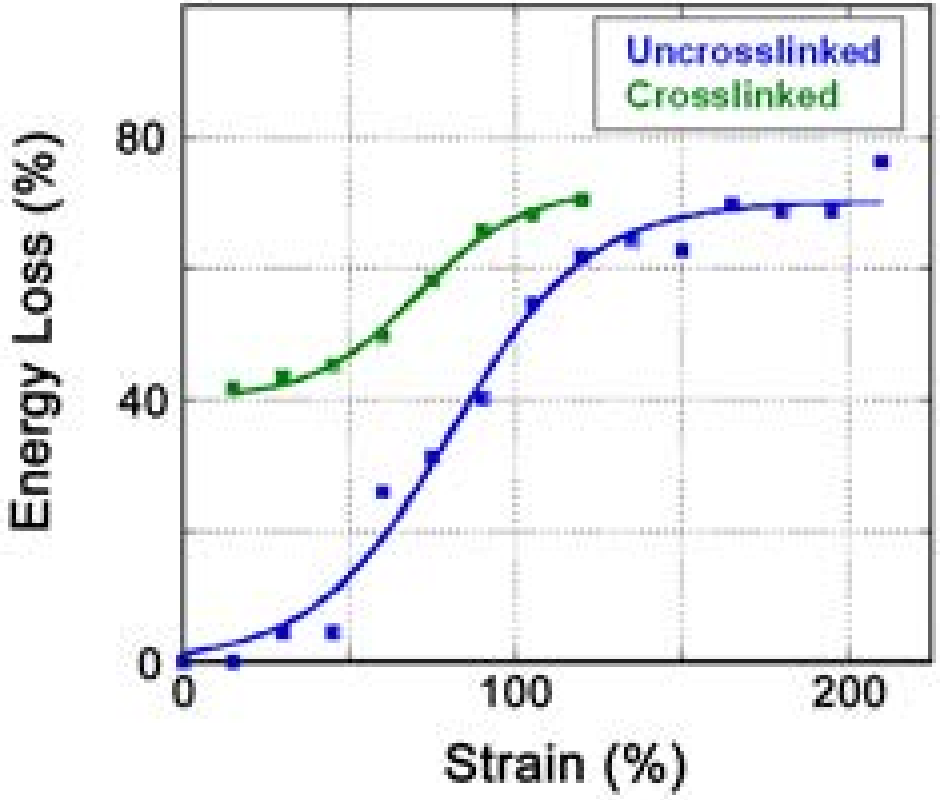
Uncrosslinked
Crosslinked
Energy Loss (%)
80
40
0
0
100
200
Strain (%)

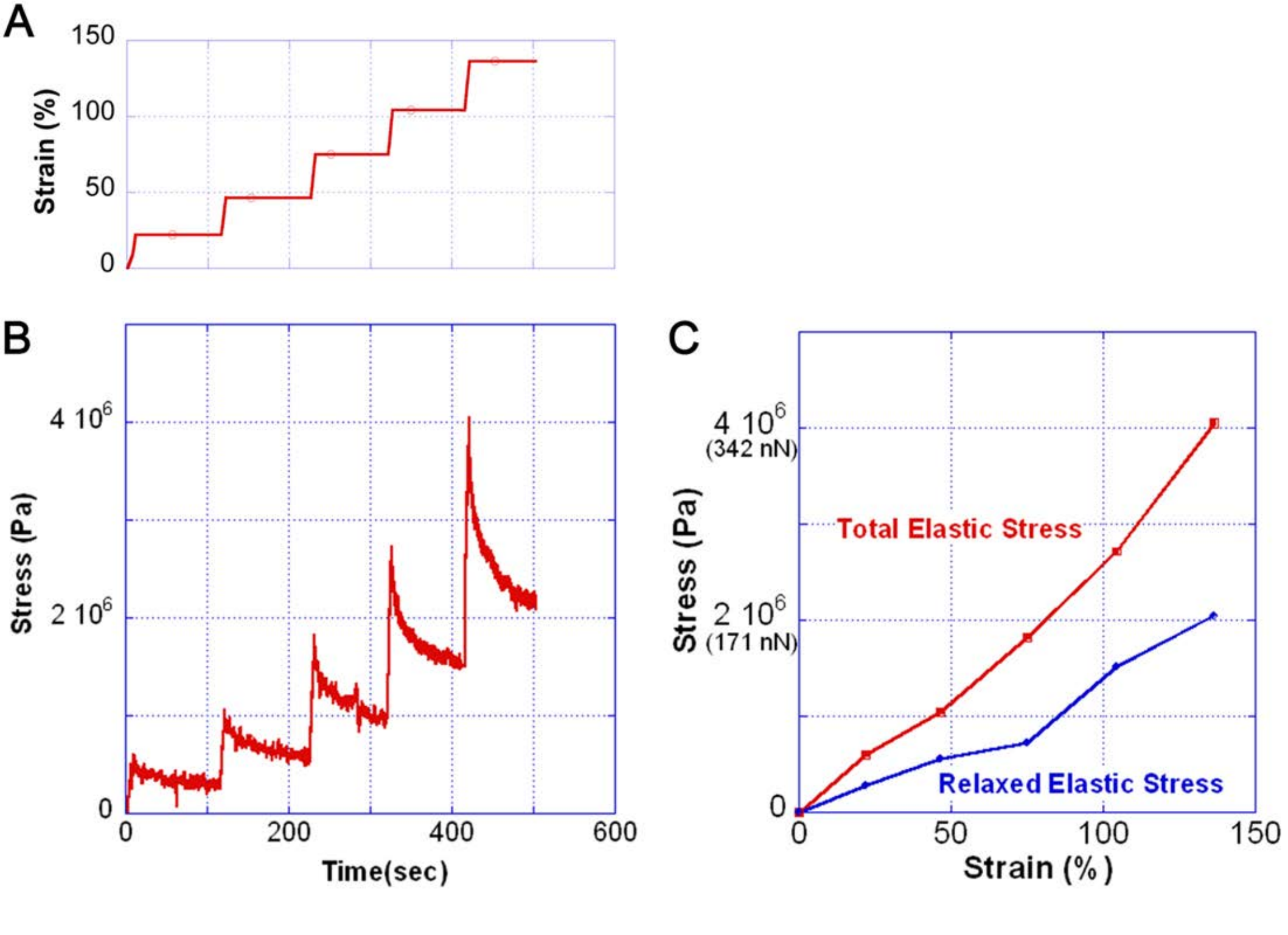
A
150
100
50
0
Strain (%)
B
4 10^6
2 10^6
0
Stress (Pa)
0
200
400
600
Time(sec)
C
4 10^6
(342 nN)
2 10^6
(171 nN)
0
Stress (Pa)
Total Elastic Stress
Relaxed Elastic Stress
0
50
100
150
Strain (%)

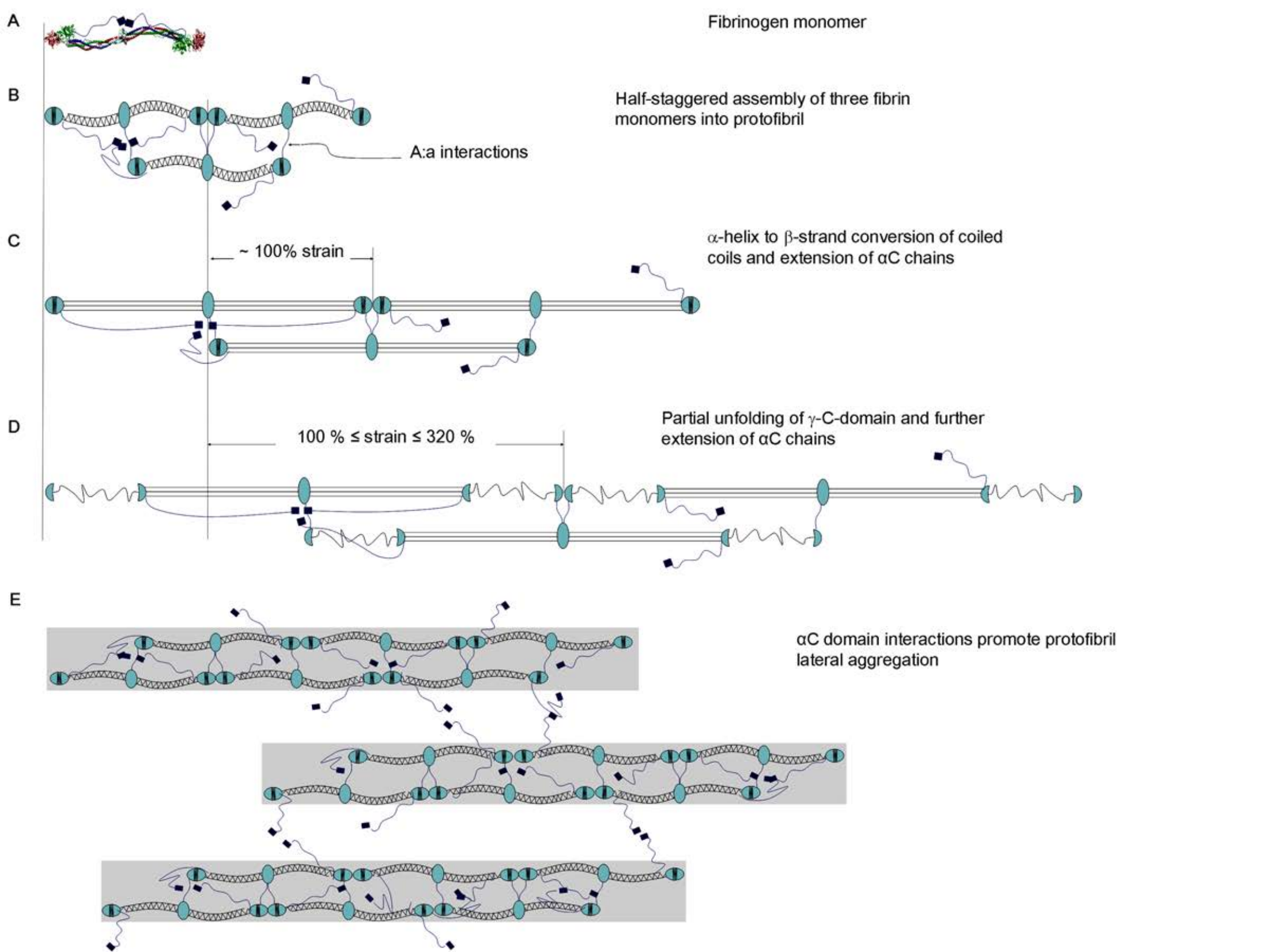
A
Fibrinogen monomer
B
Half-staggered assembly of three fibrin monomers into protofibril
A:a interactions
C
~ 100% strain
α-helix to β-strand conversion of coiled coils and extension of αC chains
D
100 % ≤ strain ≤ 320 %
Partial unfolding of γ-C-domain and further extension of αC chains
E
αC domain interactions promote protofibril lateral aggregation